REPORT

PLANAR OPTICS

Arbitrary spin-to-orbital angular momentum conversion of light

Robert C. Devlin,[1]* Antonio Ambrosio,[1,2,3,4]* Noah A. Rubin,[1]*
J. P. Balthasar Mueller,[1] Federico Capasso[1]†

Optical elements that convert the spin angular momentum (SAM) of light into vortex beams have found applications in classical and quantum optics. These elements—SAM-to–orbital angular momentum (OAM) converters—are based on the geometric phase and only permit the conversion of left- and right-circular polarizations (spin states) into states with opposite OAM. We present a method for converting arbitrary SAM states into total angular momentum states characterized by a superposition of independent OAM. We designed a metasurface that converts left- and right-circular polarizations into states with independent values of OAM and designed another device that performs this operation for elliptically polarized states. These results illustrate a general material-mediated connection between SAM and OAM of light and may find applications in producing complex structured light and in optical communication.

ircularly polarized light carries spin angular momentum (SAM) (1) of $\pm\hbar$ per photon depending on the handedness (where h is Planck's constant h divided by 2π), whereas the most general state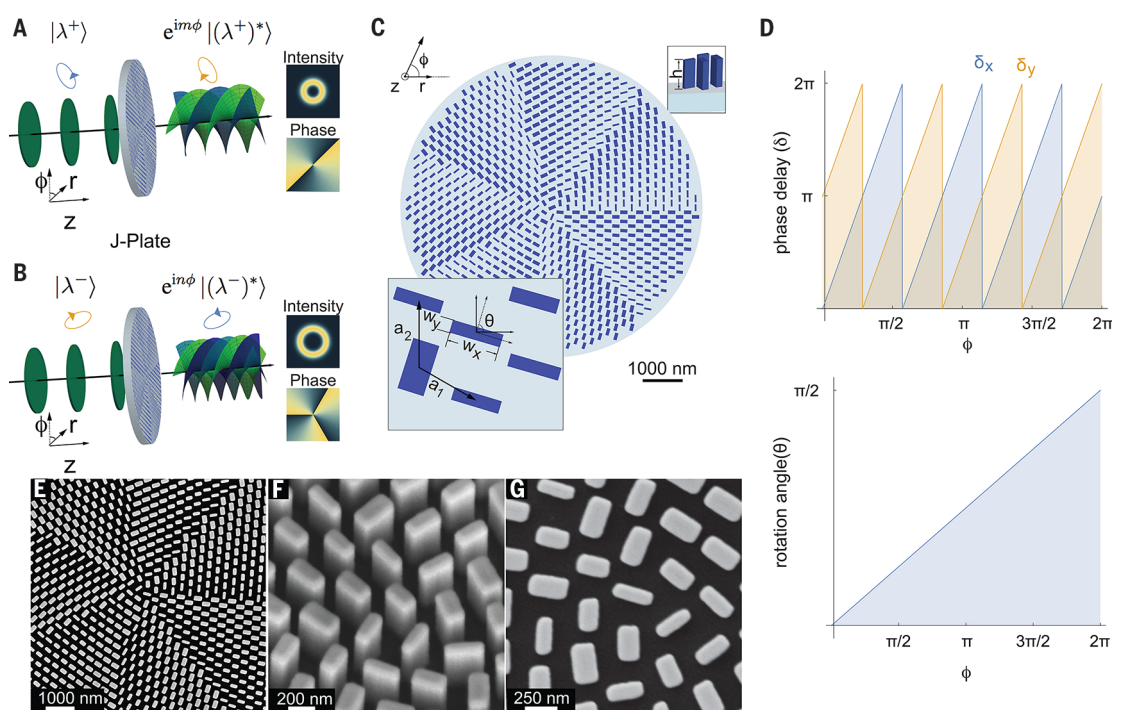 of polarization (elliptical) is a superposition of the two. Electromagnetic fields with an azimuthal phase dependence $\exp(i\ell\phi)$, where ℓ is any integer, also carry orbital angular momentum (OAM) (2). Such beams (optical vortices) exhibit ℓ multiples of 2π in phase around the azimuth with an undefined phase at the center, resulting in a "doughnut" intensity profile (3). In contrast to SAM, the OAM can take any integer value in $[-\infty, +\infty]$ corresponding to $\ell\hbar$ OAM per photon (4). A paraxial, circularly polarized helical beam has been shown to carry a total angular momentum (TAM) $J = (\sigma + \ell)\hbar$, where $\sigma = \pm1$, per photon ($2, 5, 6$).

In the more than 25 years since the discovery of light's OAM (2), optical vortices have led to a deeper understanding of light and a number of applications (7). Classical applications include optical communication ($8, 9$), micromanipulation (10), and superresolution imaging (11). The quantum nature of light's OAM has been exploited through entanglement ($12, 13$) and allows for quantum protocols with higher-dimensional quantum states (14). OAM beams may be generated in various ways: laser mode conversion (15), forked holograms (16), spiral phase plates (17), and spatial light modulators. These techniques rely on introducing a phase discontinuity in the wavefronts but generally have no connection between the SAM and OAM.

By contrast, geometric phase elements provide a direct connection between optical SAM and OAM (18). These devices are composed of identical elements with spatially varying orientation and are referred to as q-plates (19). They perform the transformation $|L\rangle \rightarrow e^{i2q\phi}|R\rangle$ and $|R\rangle \rightarrow e^{-i2q\phi}|L\rangle$, where the left and right circular polarizations are converted to output states with opposite spin and $\pm2q\hbar$ OAM. This is called spin-orbit-conversion (SOC). In addition to fundamentally connecting the SAM and OAM of light, these

Fig. 1. Arbitrary spin-to-OAM conversion. (**A**) Schematic of the concept for arbitrary SOC. Light with an arbitrary spin state (elliptical polarization), $|\lambda^+\rangle$, propagating along the z axis is incident on the J-plate. The J-plate imprints a helical phase profile on the output beam, resulting in OAM $m\hbar$, where m is any integer, and flips the handedness of the incident polarization. (**B**) For light incident on the same device with an orthogonal polarization state $|\lambda^-\rangle$, the device imprints OAM of $n\hbar$, where in general n is independent of m and again flips the handedness of the polarization. (**C**) Schematic of typical J-plate design used to carry out the function in (A) and (B). The units have a given height, h (top inset), and by changing their width along the x– and y– directions, w_x and w_y (bottom inset), the structures implement phase shifts given by δ_x and δ_y, respectively. Each unit is also allowed to have an independent orientation angle, θ. (**D**) Required phase shifts, δ_x and δ_y (top) and rotation angle (bottom) as a function of the azimuthal coordinate ϕ. The particular case plotted here is for designed input spin states that are left- and right-circularly polarized and for OAM states $m = |+3\rangle$ and $n = |+4\rangle$. (**E** to **G**) Scanning electron micrographs (SEMs) of fabricated device for the case of mapping from circularly polarized states to helical beams with OAM values of $m = |+3\rangle$ and $n = |+4\rangle$. The SEMs show (E) a top view, (F) angled view, and (G) zoomed view of the device center.

devices have broadened the applications of optical OAM, including its direct generation from laser cavities (20) and new quantum devices (21). Because of the symmetry of the design (only the constituent elements' rotation angles vary), all SOC demonstrated thus far have two inherent limitations. First, the output OAM states are not independent; they are constrained to be conjugate values ($\pm 2qh$). Second, the mapping from SAM is limited to circular polarizations—only two of an infinite set of possible polarizations.

Here, we demonstrate the design of an optical element that overcomes these limitations and provides conversion from any orthogonal polarizations to completely independent OAM states. We refer to this as arbitrary SOC because there are no restrictions on the two orthogonal input SAM states and output OAM states. This is in contrast to previous SOC devices that have used "arbitrary" to mean a device with any value of conjugate OAM (22) while still having the limitations detailed above. We implemented this design using metasurfaces because of their ability to control polarization and phase (23, 24). However, this could be realized with any medium that allows birefringence, absolute phase shift, and retarder orientation angle to vary spatially. We examined the output fields of the device and show that this technique provides for arbitrary superpositions of two TAM states. Because of its ability to map an arbitrary input SAM to two arbitrary output TAM states (where TAM is typically represented by the variable J), we refer to this device as a J-plate.

A schematic of the mapping carried out by the J-plate is shown in Fig. 1, A and B. We consider an incident paraxial beam propagating along the $+z$ direction. If the incident beam is in some arbitrary polarization state $|\lambda^+\rangle$, which in general is a superposition of spin eigenstates, we require the device to perform the transformation

$$|\lambda^+\rangle \rightarrow e^{im\phi}|(\lambda^+)^*\rangle \qquad (1)$$

that is, the output $|(\lambda^+)^*\rangle$ has opposite-handedness (24, 25), and the beam has acquired an azimuthally dependent phase factor $e^{im\phi}$, where m is any integer (Fig. 1A). The output beam has m helically intertwined phase fronts (mh OAM) and an annular intensity profile (Fig. 1A, right inset). If a beam in the orthogonal SAM state, $|\lambda^-\rangle$, is incident on the same device, we require that it yields an independent OAM state. This is shown in Fig. 1B, where the mapping is

$$|\lambda^-\rangle \rightarrow e^{in\phi}|(\lambda^-)^*\rangle \qquad (2)$$

[1]The Harvard John A. Paulson School of Engineering and Applied Sciences, Harvard University, Cambridge, MA 02138, USA. [2]Center for Nanoscale Systems, Harvard University, Cambridge, MA 02138, USA. [3]Department of Physics, Harvard University, Cambridge, MA 02138, USA. [4]Consiglio Nazionale delle Ricerche–Istituto Superconduttori, Materiali Innovativi e Dispositivi, Università degli Studi Napoli, Complesso Universitario di Monte Sant'Angelo, Via Cintia, 80126, Italy.
*These authors contributed equally to this work.
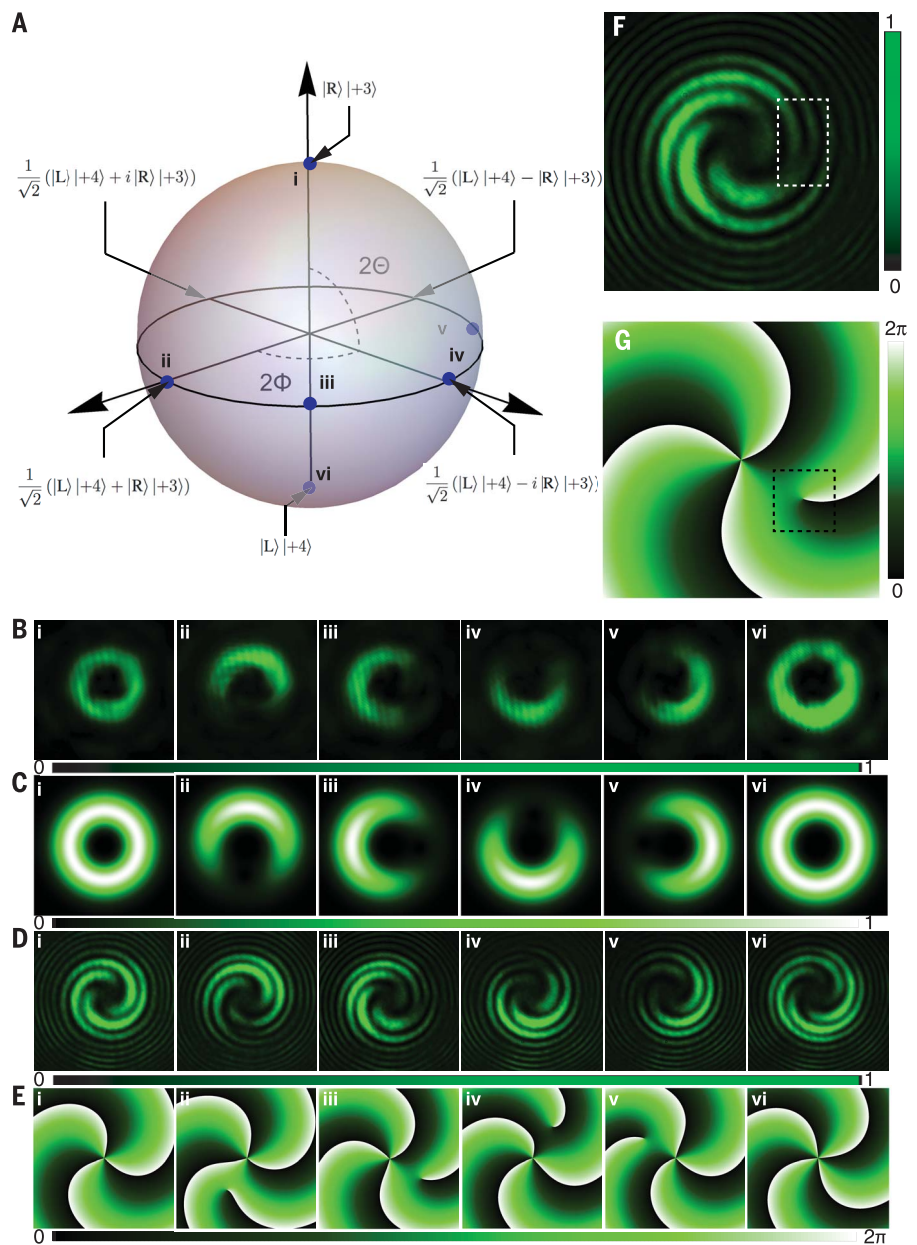†Corresponding author. Email: capasso@seas.harvard.edu

Fig. 2. Experimental demonstration of mapping from circular polarizations to two beams with arbitrary values of OAM. (A) HOPS representing all possible spin and orbital angular momentum states produced by a device that carries out the mapping $|R\rangle \rightarrow |L\rangle |+4\rangle$ and $|L\rangle \rightarrow |R\rangle |+3\rangle$. (B to E) Measured and calculated output states of the device. The output states are produced by using incident polarizations including left- and right-circular polarizations and four different linear polarizations. The states in (B) to (E), i to vi, are marked as blue circles on the HOPS in (A). (B) Measured and (C) calculated intensity of the output states. Scale bar below shows normalized intensity. (D) Measured interference and (E) calculated phase of output states. Scale bars below show (D) relative intensity and (E) the phase. (F and G) Expanded view of measured interference and calculated phase of intensity of output state in (D), iii, and (E), iii. The dashed boxes highlight an additional vortex that results from the equal superposition of $|+3\rangle$ and $|+4\rangle$ states. This vortex results in (F) an off-axis fork in the interference pattern corresponding to (G) an additional off-axis 0 to 2π phase jump. The scale bar shows the value of phase. The details of these measurements are described further in supplementary text S6.

The output has acquired an azimuthal phase factor of $e^{in\phi}$ (nh OAM), independent of m.

Implementing this mapping amounts to finding a single Jones matrix (24) that will act independently on the two input SAM states. First, we consider the two arbitrary, orthogonal polarization states introduced above, in the linear polarization basis

$$|\lambda^+\rangle = \begin{bmatrix} \cos\chi \\ e^{i\delta}\sin\chi \end{bmatrix} \quad |\lambda^-\rangle = \begin{bmatrix} -\sin\chi \\ e^{i\delta}\cos\chi \end{bmatrix} \qquad (3)$$

where χ and δ set the polarization states. To implement Eqs. 1 and 2, the case of arbitrary SOC, we can show (25) that the required matrix is

$$J(\phi) = e^{i\delta} \begin{bmatrix} e^{i\delta}(e^{im\phi}\cos^2\chi + e^{in\phi}\sin^2\chi) & \frac{\sin2\chi}{2}(e^{im\phi} - e^{in\phi}) \\ \frac{\sin2\chi}{2}(e^{im\phi} - e^{in\phi}) & e^{-i\delta}(e^{im\phi}\sin^2\chi + e^{in\phi}\cos^2\chi) \end{bmatrix} \quad (4)$$

where m and n are any integer that set the output OAM, and ϕ is the azimuthal angle. This matrix provides a general mapping from orthogonal SAM to independent OAM states. It is easily found that $J(\phi)|\lambda^+\rangle = e^{im\phi}|(\lambda^+)^*\rangle$ and $J(\phi)|\lambda^-\rangle = e^{in\phi}|(\lambda^-)^*\rangle$, as desired [a derivation of general outputs from the J-plate is provided in (25)].

We must translate this matrix into the design of an optical element. The eigenvectors and eigenvalues of J (Eq. 4) yield the required fast axis orientation angle and phase shifts, respectively, as a function of ϕ [(25), section 1]. No traditional optical element can provide the required controllable and continuous spatial variation of phase shifts, birefringence, and orientation angle of the fast axis. Metasurfaces, however—which are composed of subwavelength-spaced, birefringent phase-shifters—allow for such control. This concept is illustrated in Fig. 1C. Nanostructures are arranged periodically in two dimensions with a fixed height h (Fig. 1C, top inset), whereas the phase shifts δ_x and δ_y on light linearly polarized along the elements' symmetry axes are controlled by varying the dimensions w_x and w_y. The orientation angle of each element θ can also be independently varied (Fig. 1C, bottom inset). An important distinction compared with SOC based on the geometric phase alone is that both the phase shifts and orientation angles vary as a function of ϕ; they are both spatially inhomogeneous, thus decoupling the polarizations of the input states and the charges of the output states.

For circular polarization, $\chi = \pi/4$ and $\delta = \pi/2$ and for any values of m and n, we can find analytical solutions for the required phase shifts and orientation angles as a function of ϕ,

$$\theta = \frac{1}{4}(m - n)\phi \quad (5)$$

$$\delta_x = \frac{1}{2}(m + n)\phi \quad (6)$$

$$\delta_y = \frac{1}{2}(m + n)\phi - \pi \quad (7)$$

In Fig. 1D, we plot these equations as a function of ϕ for $m = +3$ and $n = +4$. We plot the variation of the phase shifts δ_x and δ_y, modulo 2π (Fig. 1D, top). We clearly see $(m + n)2\pi$ phase rollovers, also observed in the device design itself (Fig. 1C). For the more general case of elliptical polarizations, the solutions do not yield succinct expressions and must be calculated for specific values of m, n, χ, and δ.

We fabricated the designed devices using a process detailed elsewhere (26). This process
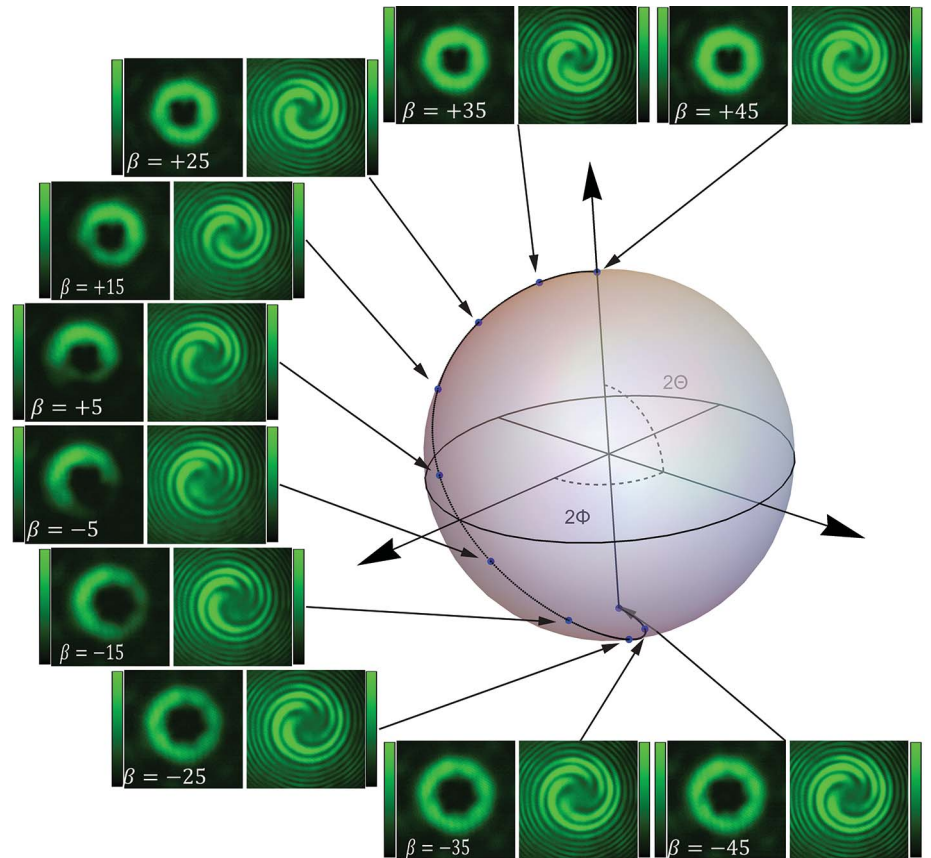

Fig. 3. Evolution of device output along a path on the HOPS. The images show measured output intensities (left) and interference (right) for the device in Fig. 2, as the angle of the fast axis of a QWP is varied in front of a horizontally polarized laser. The QWP is placed in front of the J-plate device. The QWP angle is varied from β = 45° to −45°, which transfers the output state from the north pole to the south pole while continuously changing the superposition state as $|\Psi(\beta)\rangle = \cos(\beta + \frac{\pi}{4}) e^{-i(\beta + \frac{\pi}{4})}|L\rangle|n\rangle + \sin(\beta + \frac{\pi}{4}) e^{i(\beta - \frac{\pi}{4})}|R\rangle|m\rangle$ [derivation is provided in (25)]. The QWP angle for each intensity and interference image is displayed in the bottom left. The scale bars for the normalized intensity (left) range from 0 to 1. The resulting path taken on the HOPS is shown as the black line, and the blue circles correspond to the measured points.

allows us to produce devices with high fidelity and high efficiency that operate at visible wavelengths (27, 28), with TiO$_2$ as a material platform. The devices were optimized to operate at a wavelength of 532 nm, but this design principle can be applied to any wavelength. To fully characterize a beam with OAM, its intensity and phase distributions need to be measured. Thus, we carried out interference measurements in a Mach-Zehnder configuration (fig. S1) [(25), sections 5 and 6].

To provide the most direct comparison to geometric-phase SOCs, we first demonstrate a device that converts from circularly polarized input states to two output-independent OAM beams. We chose the specific mapping to be $|R\rangle \rightarrow |L\rangle|+4\rangle$ and $|L\rangle \rightarrow |R\rangle|+3\rangle$, as in Fig. 1. We write the azimuthal phase factor $e^{im\phi}$ as $|m\rangle$ for brevity and to highlight that the J-plate output is a TAM state, a direct product between SAM and OAM states.

The set of outputs from this J-plate can be represented on a sphere whose poles are the two

output TAM states, and all other points are superpositions of these two states. This sphere that combines both SAM and OAM is called the higher-order Poincaré sphere (HOPS) (29) in contrast to the traditional Poincaré sphere. The HOPS for the case above is shown in Fig. 2A. The poles correspond to $|R\rangle|+3\rangle$ and $|L\rangle|+4\rangle$. All other outputs correspond to a point on the HOPS represented by the angular coordinates Φ and Θ (Fig. 2A).

Measured and calculated results verifying the operation of the J-plate are shown in Fig. 2, B to E. The labels i to vi correspond to the states indicated by the blue circles on the HOPS of Fig. 2A. The measured and calculated intensities for incident left and right circularly polarized light are shown in Fig. 2B, i and vi, and Fig. 2C, i and vi, respectively. These intensity profiles are single-ringed annuli with zero intensity as $r \rightarrow 0$. The measured interference pattern corresponding to the intensities in Fig. 2B, i and vi, are shown in Fig. 2D, i and v. We observed three and four arms in the spiral interference patterns that converge
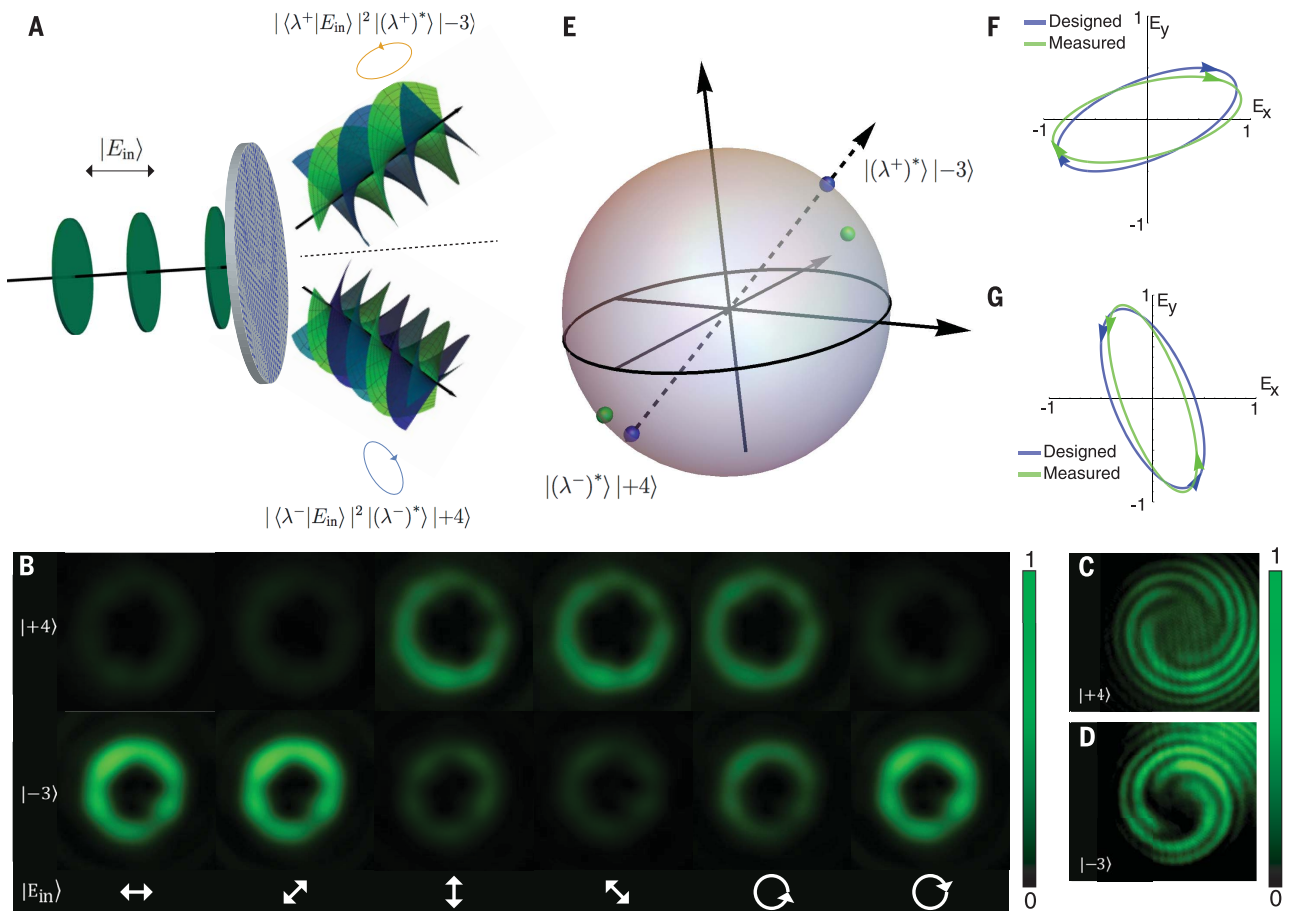
Fig. 4. Demonstration of generalized SOC. (**A**) Schematic diagram of the device that maps elliptically polarized input states to two independent states of OAM. An input beam with polarization state $|E_{in}\rangle$ is incident on the J-plate and is mapped to a superposition of OAM states, where the weights are given as a projection of the input polarization onto the two designed eigen-polarizations. An additional constant phase gradient is added to the device so that the two output states are also spatially separated by an angle of ±10°. (**B**) Stokes polarimetry to measure the eigen-polarizations. The beam intensities are shown for the two OAM states, $|+4\rangle$ and $|-3\rangle$, with the input polarization corresponding to each set of images shown at the bottom. (**C** and **D**) Interference pattern for the $|+4\rangle$ and $|-3\rangle$ states collected at angles ±10° from the z axis. The number of arms in the corresponding spiral interference patterns are (C) 4 and (D) 3, indicating that the output beams have the designed values of OAM. The sense of rotation of the spirals, however, is opposite for (C) and (D) because of the opposite-handedness of the two states. (**E**) Designed (blue) and measured (green) polarization of the output states on the HOPS. (**F** and **G**) The designed (blue) and measured (green) polarization ellipses for the input states $|\lambda^+\rangle$ and $|\lambda^-\rangle$, respectively.

on the beam axis. Shown in Fig. 2E, i and vi, are the calculated phase distribution of the two states, which have 3 and 4 multiples of 2π around the azimuth. This is consistent with the two being pure OAM states and consistent with the two designed output states for this J-plate, $|+3\rangle$ and $|+4\rangle$. These values are not conjugate.

We also examined equally weighted superpositions of the design states. To produce these states, we illuminated the J-plate with linearly polarized light. Changing the angle of the linear polarization introduces a phase shift between the $|R\rangle|+3\rangle$ and $|L\rangle|+4\rangle$ TAM states and changes longitude on the equator on the HOPS. The measured intensity for these cases are shown in Fig. 2B, ii to v. Because these states are a superposition of two beams with different OAM, we expect an additional $|m-n|$ zeros to develop in the intensity away from the beam center ($|3-4|=1$ here) (30). We observed an additional zero at a radially off-axis position,

as shown in Fig. 2B, ii to v, and Fig. 2C, ii to v. This intensity zero is also an optical vortex, and we expect m vortices at the beam center and $|m-n|$ vortices off-axis (30). This is consistent with our observations from the interference measurements and phase calculations, Fig. 2D, ii to v, and Fig. 2E, ii to v. As we change the angle of the linear polarization, all features rotate (corresponding to moving from ii to v in Fig. 2, B to E). We can understand this by noting that the relative phase changes the angle at which destructive interference between the OAM modes occurs; the positions of the intensity minima agree with quantitative expectations (30). Expanded views of one of these equal superpositions are shown in Fig. 2, F and G.

We have verified that the device produces two independent TAM states and have shown the effect of a phase difference between equal superpositions of the $|R\rangle|+3\rangle$ and $|L\rangle|+4\rangle$ TAM states. We can also continuously vary the super-

position of these states in both magnitude and phase. The continuous evolution from the $|R\rangle|+3\rangle$ to $|L\rangle|+4\rangle$ state is depicted in Fig. 3 as a function of changing input polarization to the J-plate. The path taken on the HOPS is shown as the black line in Fig. 3 and winds from the north pole, $|R\rangle|+3\rangle$, to the south pole, $|L\rangle|+4\rangle$, as a quarter-waveplate (QWP) is rotated in front of the device. The measured intensity and interference images for 10 input polarizations are shown in Fig. 3. As the polarization is changed, the interference pattern, initially composed of three on-axis spiral arms, develops an extra vortex at the periphery of the image, which circles inwards and ultimately becomes an additional arm in the spiral interference pattern, indicating that the state now has an OAM of $|+4\rangle$.

Although this case is relatively simple, we can create outputs with any two OAM values (figs. S2 to S4) (25). In addition to producing an arbitrary TAM state with polarization-controllable phase

RESEARCH | REPORT

and amplitude, we can see from Figs. 2 and 3 that this device also allows us to produce and control complex spatial intensity profiles (fig. S2).

We now consider the most general case of SOC: a mapping from arbitrary, orthogonal SAM states (elliptical polarizations) to two independent output TAM states. For this demonstration, we chose input polarizations in Eq. 3 corresponding to $\chi = \pi/6$ and $\delta = 3\pi/10$ and chose OAM states of $m = -3$ and $n = +4$. A schematic of the device that implements this mapping is shown in Fig. 4A. In addition to the normal azimuthal phase factor, we added an additional constant phase gradient that causes each output beam to be deflected by $\pm10°$ from the z axis, respectively, in contrast to the device measured in Figs. 2 and 3. Spatially separating the two TAM states allows us to independently monitor the intensity at each output angle as the input polarization is varied. The advantage here is that we can perform Stokes polarimetry to determine the eigen-polarizations of the device and compare them with the designed elliptical eigen-polarizations (fig. S5 and supplementary text).

The results of this measurement are shown in Fig. 4, B to G. First, we must verify that the two output beams contain the designed values of OAM. The measured intensity distribution for six input polarizations is shown in Fig. 4B. We collected the images at angles of $+10°$ and $-10°$ away from the z axis corresponding to the designed OAM states of $|+4\rangle$ (Fig. 4B, top) and $|-3\rangle$ (Fig. 4B, bottom), respectively. The fact that these two beams carry the two designed, independent values of OAM is confirmed through interference measurements (Fig. 4, C and D). We observed four arms in the interference pattern of Fig. 4C, whereas three arms are shown in Fig. 4D. Additionally, being of opposite sign, the sense of rotation of the interference patterns in Fig. 4, C and D, are opposite. Thus, each order contains the designed vortex beam.

Next, we verified that the device is performing the desired SOC from specified elliptically polarized inputs to two TAM states. In Fig. 4B, one can clearly observe that the output intensities of the two beams vary with input polarization. We measured the power of each beam for each input polarization in Fig. 4B and, using Stokes polarimetry, calculated the device's eigen-polarizations (25). The HOPS corresponding to the designed device is shown in Fig. 4E. The blue circles are the two designed output TAM states, and the dashed arrow passing through the two highlights that the design polarization

states are no longer circular. The green circles are the measured polarization states, with values of $\chi = \pi/6.04$ and $\delta = 3.43\pi/10$, and closely correspond to the design polarizations. Plots of the two polarization ellipses for the designed and measured input eigen-polarizations are shown in Fig. 4, F and G, respectively. Coupled with the intensity measurements and the interference measurements, this shows that we have carried out the more general form of coupling from arbitrary SAM states to two independent TAM states.

Our design shows a general material-mediated mapping between SAM and OAM and can produce arbitrary superpositions of TAM states of light. We have demonstrated the operation of the J-plate for SOC from two input circular polarizations to two independent output states, and for input elliptical polarizations in general. In addition, we have shown that a single device may create polarization-controllable structured light, in which the input SAM and output OAM states distinctly determine the spatial intensity distributions. Such functionality would otherwise require a cascade of polarization optics.

The generalized SOC presented here may influence several fields and provides interesting research directions. The compact nature of the J-plate, consisting of only a single layer of material, enables easy integration. For example, the device could be directly integrated into a laser cavity that produces arbitrary, tunable TAM states (20). States using both SAM and OAM could potentially increase the bandwidth of optical communication. Moreover, the J-plate's complex, tunable structured light can be used for laser fabrication of materials, optical micromanipulation, and stimulated emission depletion imaging. Although classical fields are considered here, the physics will still hold at the single-photon level. Thus, the J-plate can provide a new tool for quantum communication, especially in schemes that rely on transfer from polarization to OAM (13).

REFERENCES AND NOTES

1. J. H. Poynting, *Proc. R. Soc. London A Math. Phys. Eng. Sci.* **82**, 560 (1909).
2. L. Allen, M. W. Beijersbergen, R. J. C. Spreeuw, J. P. Woerdman, *Phys. Rev. A* **45**, 8185–8189 (1992).
3. J. F. Nye, M. V. Berry, *Proc. R. Soc. London A Math. Phys. Eng. Sci.* **336**, 165 (1974).
4. J. Leach, M. J. Padgett, S. M. Barnett, S. Franke-Arnold, J. Courtial, *Phys. Rev. Lett.* **88**, 257901 (2002).
5. S. M. Barnett, L. Allen, *Opt. Commun.* **110**, 670–678 (1994).
6. A. T. O'Neil, I. MacVicar, L. Allen, M. J. Padgett, *Phys. Rev. Lett.* **88**, 053601 (2002).
7. M. J. Padgett, *Opt. Express* **25**, 11265–11274 (2017).
8. G. Gibson *et al.*, *Opt. Express* **12**, 5448–5456 (2004).
9. J. Wang *et al.*, *Nat. Photonics* **6**, 488–496 (2012).
10. M. E. J. Friese, T. A. Nieminen, N. R. Heckenberg, H. Rubinsztein-Dunlop, *Nature* **394**, 348–350 (1998).
11. S. W. Hell, J. Wichmann, *Opt. Lett.* **19**, 780–782 (1994).
12. A. Mair, A. Vaziri, G. Weihs, A. Zeilinger, *Nature* **412**, 313–316 (2001).
13. R. Fickler *et al.*, *Science* **338**, 640–643 (2012).
14. A. Vaziri, G. Weihs, A. Zeilinger, *Phys. Rev. Lett.* **89**, 240401 (2002).
15. M. Beijersbergen, L. Allen, H. van der Veen, J. Woerdman, *Opt. Commun.* **96**, 123–132 (1993).
16. V. Y. Bazhenov, M. Vasnetsov, M. Soskin, *JETP Lett.* **52**, 429 (1990).
17. M. Beijersbergen, R. Coerwinkel, M. Kristensen, J. Woerdman, *Opt. Commun.* **112**, 321–327 (1994).
18. G. Biener, A. Niv, V. Kleiner, E. Hasman, *Opt. Lett.* **27**, 1875–1877 (2002).
19. L. Marrucci, C. Manzo, D. Paparo, *Phys. Rev. Lett.* **96**, 163905 (2006).
20. D. Naidoo *et al.*, *Nat. Photonics* **10**, 327–332 (2016).
21. E. Nagali *et al.*, *Nat. Photonics* **3**, 720–723 (2009).
22. F. Bouchard *et al.*, *Appl. Phys. Lett.* **105**, 101905 (2014).
23. A. Arbabi, Y. Horie, M. Bagheri, A. Faraon, *Nat. Nanotechnol.* **10**, 937–943 (2015).
24. J. P. Balthasar Mueller, N. A. Rubin, R. C. Devlin, B. Groever, F. Capasso, *Phys. Rev. Lett.* **118**, 113901 (2017).
25. More information on device design, additional demonstrations, measurements, and methods are available as supplementary materials.
26. R. C. Devlin, M. Khorasaninejad, W. T. Chen, J. Oh, F. Capasso, *Proc. Natl. Acad. Sci. U.S.A.* **113**, 10473–10478 (2016).
27. M. Khorasaninejad *et al.*, *Science* **352**, 1190–1194 (2016).
28. R. C. Devlin *et al.*, *Opt. Express* **25**, 377–393 (2017).
29. G. Milione, H. I. Sztul, D. A. Nolan, R. R. Alfano, *Phys. Rev. Lett.* **107**, 053601 (2011).
30. S. M. Baumann, D. M. Kalb, L. H. MacMillan, E. J. Galvez, *Opt. Express* **17**, 9818–9827 (2009).

Science

Arbitrary spin-to–orbital angular momentum conversion of light

Robert C. Devlin, Antonio Ambrosio, Noah A. Rubin, J. P. Balthasar Mueller and Federico Capasso

From spins to spirals
The polarization state of light can be used in imaging applications and optical communications. Light can also be structured into vortices that carry optical angular momentum, which can be used for micromanipulation and enhancing the capacity of optical communication channels. Devlin *et al.* present a metasurface converter for optical states that transforms polarization states into optical angular momentum states. The coupling between arbitrary spin and optical angular momentum states of light in a compact planar structure may find applications in producing complex structured light fields.
Science, this issue p. 896

ARTICLE TOOLS	http://science.sciencemag.org/content/358/6365/896
SUPPLEMENTARY MATERIALS	http://science.sciencemag.org/content/suppl/2017/11/01/science.aao5392.DC1
REFERENCES	This article cites 27 articles, 3 of which you can access for free http://science.sciencemag.org/content/358/6365/896#BIBL
PERMISSIONS	http://www.sciencemag.org/help/reprints-and-permissions

Use of this article is subject to the Terms of Service